International Journal of Advanced Geosciences, 14 (2) (2026) 111-123

International Journal of Advanced Geosciences

Website: www.sciencepubco.com/index.php/IJAG
https://doi.org/10.14419/qpxcja32
Research paper

Geophysical Characterization of Aquifer Potential Regions Using Multi–Criteria Decision Analysis (MCDA) Process: A Case Study of Gabasawa and its Environs Kano State, Nigeria

Samir Auwalu [1] *, Muhammad Saleh [2], Maitama A. Yusuf Hotoro [3], Hamza Salihu Adamu [4]

[1] Department of Physics, Jigawa State College of Remedial & Advanced Studies, Babura, Nigeria
[2] Department of Physics, Bayero University, Kano, 700241 Kano, Nigeria
[3] Department of Physics, Aliko Dangote University of Science and Technology, Wudil, Nigeria
[4] Energy Commission of Nigeria, Abuja
**Corresponding author E-mail: samirundudu@yahoo.com*

Received: 7 Aug 2026, Accepted: 22 Oct 2026, Published: 10 Nov 2026

Abstract

The study aims to determine the aquifer characteristics of Gabasawa and its environs using multi-criteria decision analysis to provide sufficient information on groundwater potential zones. Magnetic, elevation, and electromagnetic data were acquired using Magneto-meter and Audio Magnetotelluric device. The acquired data were reduced and modelled using Surfer 25.0 and Oasis Montaj 8.4. Source Parameter Imaging was used to calculate depth around the area. Deeper depths with values ranging from 42.0 to 120.1m were isolated for groundwater exploitation. Slope was deduced from the elevation grid. Centre for Exploration and Target Analysis was used to obtain magnetic and Elevation Lineaments. The lineaments were joined to form lineament intersections. Predominant lineaments were observed in North-East and South-west locations; this showed a a tendency for surface water and groundwater accumulation. These lineaments and intersections were transformed into lineament density grids. These lineament densities, coupled with source parameter imaging, elevation, and slope , were resampled and reclassified into thematic layers. Multi-criteria decision analysis was used to calculate the weight of each thematic layer. The sum of the products of the thematic layer and their respective weight were obtained using the weight overlay menu of ArcGIS 10.8, leading to the development of groundwater potential zones map. The groundwater potential zones map was classified into five regions of very high, high, moderate, low, and very low groundwater potential zones with area coverage of 0.4041km2, 2.1772 km2, 2.8962 km2, 1.9562 km2, and 0.0024 km2 , respectively. Electromagnetic data analysis revealed the area to be underlain by four lithological layers: topsoil, silty sand, laterite, gravels, and sandstone, with the fourth layer inferred as the aquifer zone. The groundwater potential zones were validated using existing hydrogeological data and aquifers delineated from interpreted Electromagnetic data. It was observed that 92.86% of the plotted points and zones falls within regions ranging from very high to moderate groundwater potential zones.

Keywords: *Aquifer; Groundwater Potential; Ground Magnetic; Elevation; Electromagnetic; Lineament; Slope; Source Parameter Imaging.*

1. Introduction

Groundwater constitutes approximately 30–40% of world portable water source and necessary in providing water security, especially in regions with limited or no surface water [1]. In sub-Saharan Africa regions, 75% of water used for domestic, agricultural, and industrial purposes comes from groundwater [2]. In semi–arid regions like Nigeria, with unpredictable rainfall, high evaporation, and seasonal surface water flow, which create high water scarcity, a reliable option is groundwater [3]. Nigeria's population is estimated to exceed 230 million people, with an increase rate of approximately 2.6% per annum; this imposes pressure on its water resources, with per capita freshwater availability declining below the United Nations threshold for water security in northern states [4].
Locating groundwater in basement complex rock terrains is quite challenging [5]. In crystalline basement areas, groundwater is found in weathered, fractured, faults, and joints, basically in discontinuous layers [6]. Basement complex rock terrains have highly heterogeneous hydrogeological properties, indicating groundwater uncertainty [7]. Consequently, basement complex terrains have a very high rate of borehole failure, with success rates as low as 40–60% in some parts of the Nigerian basement complex regions due to inadequate geophysical characterization [8]. The economic and social costs of abortive boreholes are substantial, including financial losses, abandonment of

Copyright © Samir Auwalu et al. This is an open access article distributed under the Creative Commons Attribution License, which permits unrestricted use, distribution, and reproduction in any medium, provided the original work is properly cited.

community water projects, and perpetuation of water-related health risks and gender inequality as women and girls bear responsibility for water collection from distant, often unsafe sources [9].

Gabasawa and its environs are a typical example of all these challenges. The area sits on the Northern Nigerian Basement Complex rocks composed of migmatite gneiss, porphyritic granites, and older granite, younger metasediments, and volcanic rocks of the Precambrian [10]. The region falls within the semi-arid tropical climate characterized by mean annual rainfall ranging from 800–1000 mm between the months of June and September, followed by an extended dry season of seven to nine months [11]. Mean annual temperatures range from 26°C to 33°C, with maximum exceeding 40°C during the hot season between March and May. Evapotranspiration rates typically exceed precipitation for most of the year, creating a negative water balance that limits natural groundwater recharge and increases reliance on stored groundwater resources [12]. The vegetation is tropical savannah, characterized by sparse shrub cover and isolated trees, with limited organic matter to enhance soil infiltration capacity [13].

Recently, Gabasawa and its surrounding population are growing rapidly due to natural increase and rural - urban migration seeking economic opportunities in Kano State's expanding agricultural and commercial sectors [14]. This demographic growth has intensified pressure on existing water supply infrastructure. Most communities rely on hand-dug wells, seasonal ponds, and a limited number of boreholes, many of which experience reduced yields or complete failure during the dry season [15]. The combination of unfavorable hydrogeological conditions, limited technical capacity for groundwater exploration and insufficient financial resources for systematic geophysical investigations has resulted in frequent borehole failures and persistent water insecurity [16].

Communities around the study area relied heavily on local knowledge, geological observations, and wildcat drilling in siting boreholes rather than hydrogeological and geophysical characterization [17]. These approaches are unreliable and unrepeatable for sustainable groundwater development at community scale. The absence of systematic geophysical investigations prior to drilling has been identified as a primary factor contributing to the high rate of borehole failures in basement terrains across Nigeria [18]. Therefore, there is an urgent need for a structured and evidence-based methodology that can characterize aquifer potential at multiple scales from regional reconnaissance to local-scale validation, to guide drilling [19].

2. Methods

2.1. Location and hydrogeology of the study area

The study area is located within Gabasawa Local Government Area of Kano State with an area coverage of approximately 8km^2 bounded by latitude $8^0$53′24′′E to $8^0$54′58.20′′E and $12^0$10′22.8′′N to $12^0$11′55.33′′N with an elevation varying from 405.23m to 420.84m above sea level. The area has an average temperature of 33^0C and a wind speed of 10km/h [11]. Major towns include Sabon Garin Kumbo, Kumbo, Mazangudu, Gabasawa and Walawa. The geology of the study area is underlain by basement complex rocks of Northern Nigeria and sedimentary rock of the chad formation in the northeastern region of the state. The basement complex rock comprises of the older and younger granite, migmatite-gneiss and schist [20]. Hydrogeologically, the occurrence of water-bearing zones and fractures in the area is within the highly decomposed to partially weathered basement rocks and fractured basement rocks, and these are found at depths in excess of 5 meters. The weathered and fractured basement rocks with a relatively thin overburden underlie the area surveyed [21].

2.2. Theoretical background

The magnetic method theories are categorized into data acquisition and data interpretation theories.

The Total Magnetic field Intensity (TMI) at a region [22] is given as

$$T = \mu_0 H(1 - k) \tag{1}$$

Where H is the magnetic field strength, k is the magnetic susceptibility, and μ_0 is the permeability.

T is subjected to polynomial fitting using the polynomial P(x, y) equation.

$$P(x, y) = a + bx + cy \tag{2}$$

Where a, b, and c are constants obtained from fitting, and x and y are geographic coordinates

In this analysis, P(x, y) is taken as the Regional Magnetic Intensity (R) that is removed from T to obtain Residual Magnetic Intensity (RMI)

$$RMI = T - R \tag{3}$$

The residual grid data were subjected to RTE using equation 1 in order to eliminate the effect of magnetic inclination in regions with low latitude by centering the peaks of the magnetic anomalies on their source body using the relation in equation 4.

$$L(\theta) = \frac{\sin(I) - i\cos(I).\cos(D-\theta)^2 x(-\cos^2(D-\theta)}{[\sin^2 I_a + \cos^2(I_a).\cos^2(D-\theta)]x[\sin^2(I) + \cos^2(I).\cos^2(D-\theta)]} \tag{4}$$

Where I is geomagnetic Inclination, D is Geomagnetic Declination, I_a is Inclination for amplitude correction.

Developed by Telford et, al. [23] the SPI method is used to calculate depth for fresh basement complex rock [24] is given by

$$D = \frac{1}{\sqrt{\left(\frac{\partial T}{\partial x}\right)^2 + \left(\frac{\partial T}{\partial y}\right)^2}} \tag{5}$$

The tilt angle [24] is given by

$$\theta = \arctan \frac{\frac{\partial T}{\partial z}}{\sqrt{\left(\frac{\partial T}{\partial x}\right)^2 + \left(\frac{\partial T}{\partial y}\right)^2}} \tag{6}$$

The pairwise comparison between a set of criteria helps make multifaceted decision [25]. First, the thorny decision-making procedure between primary parameters is transformed into a single level by a pairwise comparison matrix in equation [25]; [26].

$$A = \begin{bmatrix} a_{2i} & \cdots & a_{2n} \\ \vdots & \ddots & \vdots \\ a_{n1} & \cdots & a_{nn} \end{bmatrix} \quad (7)$$

In this judgment matrix, the elements are: The geometric average of the criteria is express in equation 8 [25]; [26]

$$W_n = \frac{G_i}{\sum_{i-1}^{n} G_i} \quad (8)$$

G_i and W_n respectively represent the geometric average and eigenvalue of the judgement of the i^{th} row. The consistency of the normalized criteria weight is assessed using equation 9 [27]

$$CR = \frac{CI}{RI} \quad (9)$$

Where CR is the consistency ratio, CI is the consistency index, and RI is the consistency ratio index. For a normalized weight to be deemed consistent, the consistency ratio CR should be lower than 0.10 [25]: [27]
The consistency index CI is expressed in equation 10 as [27]

$$CI = \frac{\lambda_{max} - n}{n-1} \quad (10)$$

λ_{max} derived is the maximum eigenvalue of the judgment matrix
The groundwater Potential Zone (GWPZ) is calculated using equation 11 [28]

$$GWPZ = \sum_{i}^{n}(x_i \times y_i) \quad (11)$$

Where x_i is the weight of each thematic layer, y_i is the corresponding thematic or raster layer, and i and n is the number of thematic layers. Surface electromagnetic waves are sent to the ground, and the propagation of electromagnetic waves in the earth and soil follows the Maxwell equation. From the Maxwell equation, the resistivity can be deduced as [22]

$$\rho = \frac{\mu_0}{\omega}\left|\frac{E}{H}\right|^2 \quad (12)$$

Where E is the electric field, H is the magnetic field, μ_0 is the permeability of free space, and angular frequency $\omega = 2\pi f$
The depth can be calculated using equation (13) given by [22]

$$d = \frac{2}{\omega}\left|\frac{E}{H}\right| \quad (13)$$

2.3. Magnetic and elevation data acquisition

GSM-19 Overhauser magnetometer was used in data acquisition for Total Magnetic Intensity (TMI) and Elevation Data across the study area. The GSM-19 magnetometer was assembled and mounted on the researcher and subsequently on other field assistants. A base station was established, and its reading was acquired. The first station TMI readings were continuously acquired by walking along the profile lines one of length 500m and coming back along profile line two also of length 500m this was repeated along profile lines 3, 4, 5, 6, 7, 8, 9 and 10. Base station readings were taken at an interval of 60 minutes. The same procedure was repeated on stations 2, 3, 4, 5, 6, 7 and 8, respectively. The TMI data obtained was downloaded from the device to a personal computer; the data was subjected to diurnal correction using GEM-Link 5.4. The corrected data was uploaded and gridded in Surfer version 30.1.218, and a TMI grid was obtained which was later transferred to the ArcGIS 10.8 environment and processed to obtain the TMI map of the area, as shown in Figure 4. The elevation data was acquired in the same manner as magnetic data and was processed in the same way as the TMI data, and the elevation map obtained is shown in Figure 5. The TMI grid obtained was filtered and modelled using Equations 2, 3, 4, 5 and 6. Regional – Residual, Reduce To Equator (RTE), and Source Parameter Imaging (SPI) grids were generated. The magnetic lineament and elevation lineament were extracted using the Centre for Exploration Target (CET) analysis menu in Oasis Montaj software. The lineaments obtained were intersected, and a lineament intersection grid was obtained. The magnetic, elevation, and lineament intersections were transformed into density maps using the spatial tool function of ArcGIS environment. The SPI, Magnetic Lineament Density (MLD), Elevation Lineament Density (ELD), Lineament Intersection Density (LID), Elevation (E) and Slope (SL) grids obtained were resampled and reclassified. After reclassification, six (6) thematic layer maps SPI, MLD, ELD, LID, E and SL were obtained.

2.4. Electromagnetic data acquisition method

The electromagnetic data acquisition was carried out using the TT electromagnetic probe of the ADMT-200S in the study area for fast data acquisition. The device was turned on, and the sensor was connected to the device and placed on the marked point on the profile. The measurement point is directly under the sensor. The placement direction of each measuring point on a survey line is consistent. The device measures the potential difference in the range of 0–200 mV with a 0.1 mV resolution. The sampling frequency is 1 Hz to 8 kHz, offering a sampling depth of about 200m [29].
To start the measurements, 10 profile lines GRWT 1 to GRWT 10 of length 64m. The ADMT smart receiver was connected to the electro-magnetic probe via a cable, and the probe was placed on the marked point along the profile line GRWT 1; the first sampling data was acquired after 2 minutes. The sensor was then moved 8m to the second marked point along the profile, and the sampling data was acquired. The same procedure was repeated at marked points 3, 4, 5, 6, 7 until the 8^{th} sampling data was collected along GRWT 1. This procedure

was repeated on profile lines GRWT 2 to GRWT 10. The sampling data acquired were inverted using an inbuilt software of the ADMT-200s.

2.5. Analytic hierarchy process (AHP) method

Adopted in this research work is the AHP using Multi-criteria Decision Analysis (MDCA); the pairwise matrix was generated using factors (criteria) SPI, MLD, ELD, LID, E and SL. With an expert opinion established by [25]. Using the factors listed, a pairwise matrix was generated in accordance to their importance relative to one another, as shown in Table 2.

Table 1: Pairwise Matrix

Factor	SPI	MLD	ELD	LID	E	SL
SPI	1.00	5.00	3.00	7.00	9.00	7.00
MLD	0.20	1.00	5.00	5.00	9.00	5.00
ELD	0.20	0.20	1.00	0.33	0.50	5.00
LID	0.20	0.20	3.00	1.00	9.00	3.00
E	0.20	0.20	3.00	0.11	1.00	3.00
SL	0.20	0.20	3.00	1.00	0.33	1.00
SUM	2.00	6.80	18.00	14.44	28.50	24.00

Table 2: Normalized Pairwise Matrix Showing the Weight, Consistency Index, Random Consistency Index and Consistency Ratio

Normalization	SPI	MLD	ELD	LID	E	SL	Average	Lambda	CI	RCI	CR
SPI	0.50	0.74	0.17	0.48	0.32	0.29	0.42	9.21	0.13	1.24	0.10
MLD	0.10	0.15	0.28	0.35	0.32	0.21	0.24	9.33			
ELD	0.10	0.03	0.06	0.02	0.02	0.21	0.05	4.01			
LID	0.10	0.03	0.17	0.07	0.32	0.13	0.14	9.09			
E	0.10	0.03	0.17	0.01	0.04	0.13	0.07	8.49			
SL	0.10	0.03	0.17	0.07	0.01	0.04	0.08	6.63			
SUM	1.00	1.00	1.00	1.00	1.01	1.00	1.00	9.21			

The pairwise matrix comparison was normalized using equation 8 as shown in Table 3; the Random Index (RI) given in [30] used to calculate the Consistency Index (CI). The Consistency Ratio (CR), Consistency Index (CI), and maximum eigenvalues of the judgment matrix shown in Table 3 were calculated using equations 9, 10, and 11. The groundwater Potential Map (GWPM) was generated by multiplying thematic layers with their respective weighted values, the products were summed up using the Raster Calculator menu in ArcGIS Environment.

3. Results and Discussions

3.1. TMI grid and elevation

Figure 1(a) shows the TMI map of the study area, the map shows variations in magnetic susceptibility across the area. The variation in magnetic strength ranges from 19484.6nT to 35694.1nT across the area. Low magnetic intensity ranging from 19484.6nT – 31411.2nT were observed in the Northeastern, Southeastern and Southwestern regions. High magnetic anomalies ranging from 33950.8 nT to 35694.1 nT were observed in the aforementioned regions. These changes in magnetic intensity give rise to discontinuities in the rocks that result in lineaments, faults, and fractures, which are good factors for groundwater accumulation.

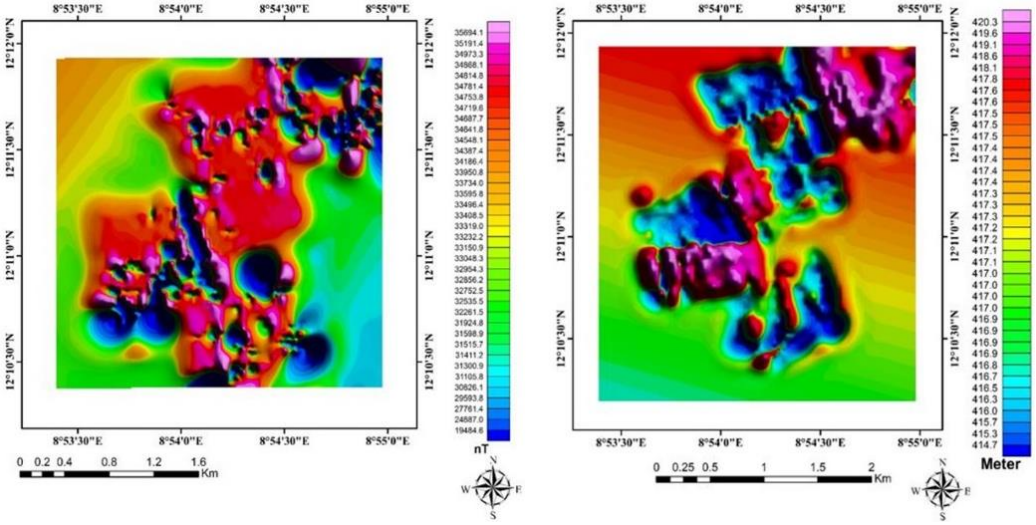


Fig. 1: (A) Total Magnetic Intensity Map of the Area (B) Elevation Map of the Area.

Figure 1(b) shows the study area elevation map; the map shows the areas of peaks and depressions above sea level. The region is categories in to three (3); the peak regions, Moderate depressions regions and high depression regions with value ranging from 417.3m to 420.3m above sea level in the NE, NW and SW part in the area, with value range of 416.9m to 417.3m above sea level in the NE, North, West SE, SW, and with value range of 414.7m to 416.8m above sea level in the NE, North, West SE, and SW respectively. These values indicate that surface water moves toward high depression regions.

3.2. Residualisation

Regional residual separation results were obtained using Equations 2 and 3. The regional – residual data obtained were gridded, and their respective maps were obtained as shown in Figure 2(a) and 2(b). The regional map shows the trends in magnetic anomalies to be from NW to SE around the areas. The residual map shows variation in the magnetic intensity around the study area. High magnetic intensity was observed to trend from north to south, other areas were seen in the NE, SE, and SW, with intensity values ranging from 1795.8nT to 4897.1nT. Intermediate to low intensities were spatially distributed in the NE, NW, SE, and SW regions with a value range of -11240nT to 1255.9nT. This change in magnetic intensity inferred the heterogeneous nature of the rocks in the region. This heterogeneous type of formation may aid groundwater accumulation.

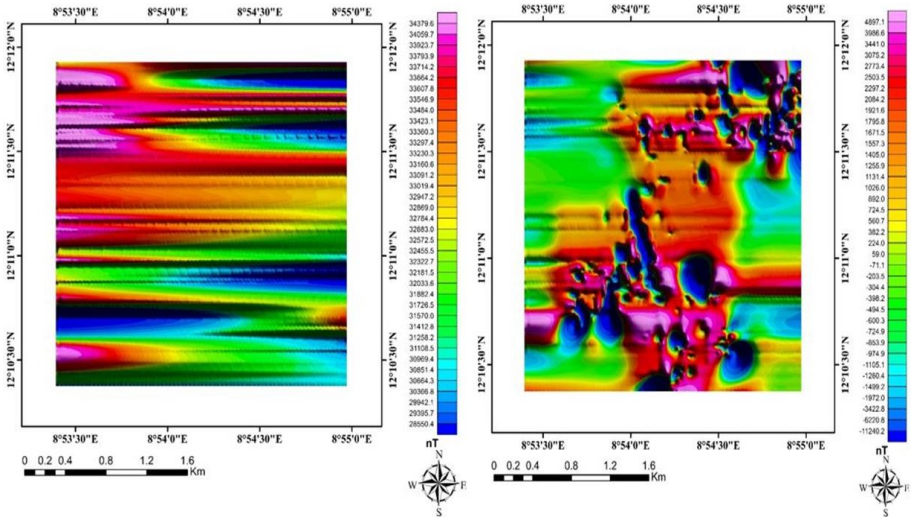


Fig. 2: (A) Regional Map of the Area (B) Residual Map of the Area.

3.3. Reduction to the equator (RTE)

Figure 3 indicates the RTE map of the study area, which shows the variation in magnetic intensity. High magnetic intensity was observed in the North, South, and in the NE, SE, and SW regions, with a value range of 1094.6nT to 4130.3nT. Intermediate to low magnetic intensity value of range -8102.6nT to 948.2nT were observed in the NE, SE, NW and SW regions of the RTE map. This discontinuity in the rock's magnetic anomalies gives rise to lineaments that aid groundwater accumulation.

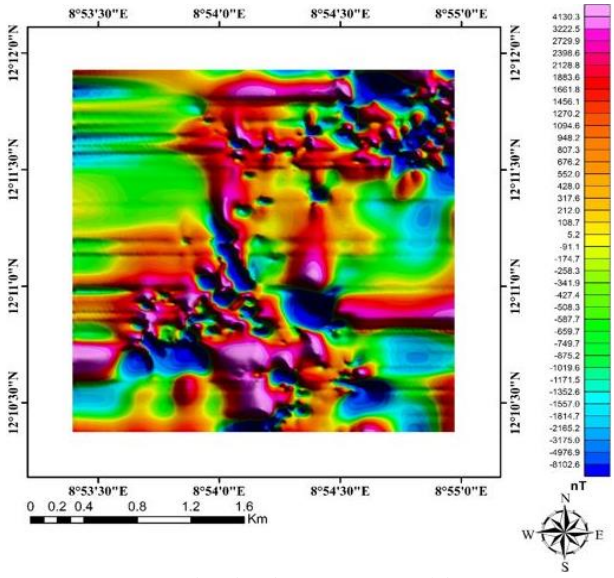


Fig. 3: Reduced to the Equator Map of the Area.

3.4. Magnetic lineaments and thematic magnetic lineament density layer

In Figure 4(a), the lineament were observed to be more predominant in the NE and SW regions, with few in the SE zone of the area. This shows that the general trend in the lineament is in the NE to SW direction. This lineament of the rocks around the area are inferred as fracture and weathered rock that serves as groundwater accumulation zones.

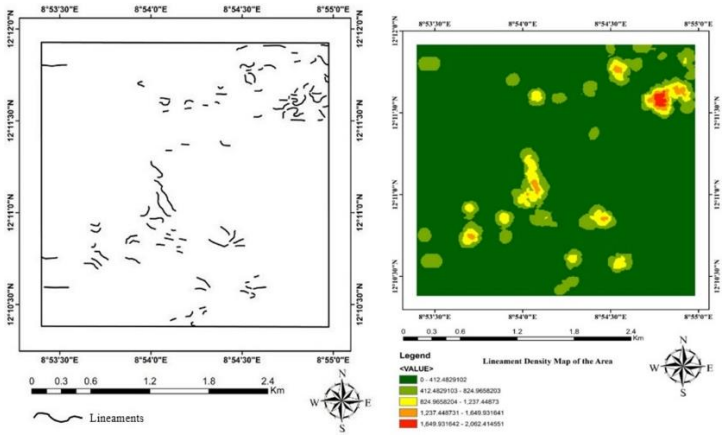


Fig. 4: (A) Magnetic Lineament Map of the Area (B) Thematic Magnetic Lineaments Density Layer Map of the Area.

Figure 4(b) show thematic magnetic lineament density of the study area. The lineament density is reclassified into five classes; each class is assigned a specific color and a number from 1 to 5. The classes ranges from very low (very low lineament density) to very high potential (very high lineament density). Classes 2, 3, and 4 are for low lineament density, moderate lineament density, and high lineament density, respectively. This thematic was assigned a weight of 24% in groundwater potential of the study area as shown in Table 4.

Table 3: List of Factors, Class, Rating and Weights

Factor	Class	Rating	Weight (%)
	12.6734 - 32.0749	1	
	32.0749 - 61.1613	2	
SPI	61.1613 - 105.9096	3	42
	105.9096 - 217.7804	4	
	217.7804 - 557.8676	5	
	0 - 121.3185	1	
	121.3185 - 388.2192	2	
MLD	388.2192 - 703.6473	3	24
	703.6473 - 1,124.2181	4	
	1,124.2181 - 2,062.4146	5	
	0 - 138.9148	1	
	138.91481 - 396.8995	2	
ELD	396.8995 - 635.0392	3	5
	635.03915 - 906.2538	4	
	906.2538 - 1,686.8228	5	
	0 - 556.7380859	1	
	556.7381 - 1,113.4762	2	
LID	1,113.4762 - 1,670.2143	3	14
	1,670.2143 - 2,226.9523	4	
	2,226.9523 - 2,783.6904	5	
	410.1186 - 414.5757	5	
	414.5757 - 416.4329	4	
E	416.4329 - 417.9716	3	7
	417.9716 - 419.6165	2	
	419.6165 - 423.6492	1	
	0.0005 - 0.4260	5	
	0.4260 - 1.3303	4	
SL	1.3303 - 2.7666	3	8
	2.7666 - 5.2667	2	
	5.2667 - 13.5650	1	

3.5. Elevation lineaments and thematic elevation lineament density map

The elevation lineaments in Figure 5(a) were extracted from the hillshade raster grid. The lineaments were also observed to trend from NE to SW of the study area. This indicates that surface water mostly flows through these regions and may serve as a good aquifer recharge zone.

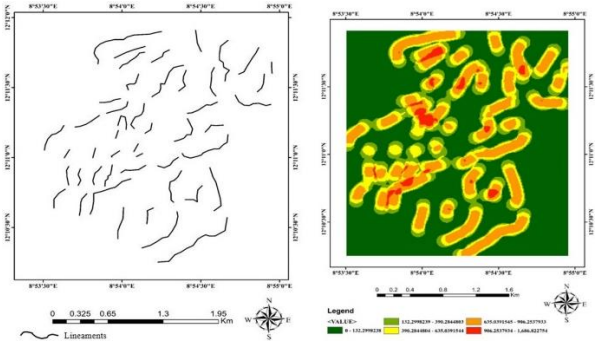


Fig. 5: (A) Elevation Lineaments Map of the Area (B) Thematic Elevation Lineament Density Layer Map of the Area.

Figure 5(b) shows the thematic layer of the lineament density of the elevation of the study area. The area was classified in five classes ranging from one (1) very low (very lineament density) to (5) very high (very high lineament density). Classes 2, 3, and 4 stand for low, moderate, and high lineament density. A weight of 5% was assigned to the elevation lineament density thematic layer in groundwater potential of the area as in Table 4.

3.6. Lineament intersections and thematic lineament intersection density layer

The lineament intersection map shown in Figure 6(a) indicates that there was an intersection of magnetic and elevation lineaments in the NE, NW, SE, and SW regions of the study area. It is inferred that areas with high lineament intersection may have high groundwater potential.

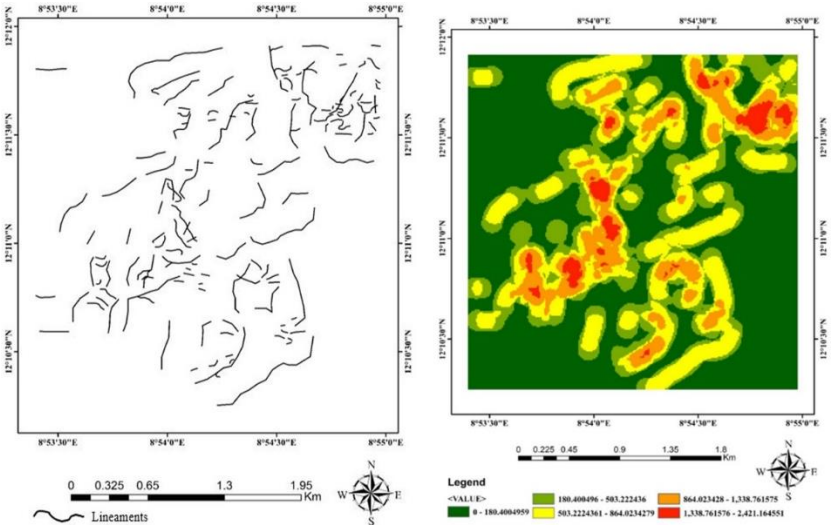


Fig. 6: (A) Lineament Intersection Map of the Area (B) Thematic Lineament Intersection Density Layer Map of the Area.

Figure 6(b) shows the thematic layer of lineament intersection density of the study area. The layer is classified in five classes ranging from 1(very low lineament intersection density) to 5 (very high lineament intersection density). Classes assigned 2, 3, and 4 fall within low, moderate, and high lineament intersection density. Thematic layer of the lineament intersection density is assigned a weight value of 14% in the groundwater potential of the study area, as shown in Table 4.

3.7. Source parameter imaging (SPI) and thematic SPI layer

Figure 7(a) is the SPI map of the study area; this map shows the depth to the magnetic source body in the area. The area depth is categorized into three (3) regions: deeper depth source, intermediate source, and shallow source region. The deeper depth region of depth value ranging from 42.0m to 120.1m were observed NE, SE, NW and SW. Intermediate depth regions with values ranging from 39.7m to 17.3m were observed around the deeper depth. Shallow depth regions were observed in the NE, NW, SE, and SW parts with values ranging from 16.4m to 10.1m. The deeper regions are presumed to be area of high groundwater potential zones show in Table 4.

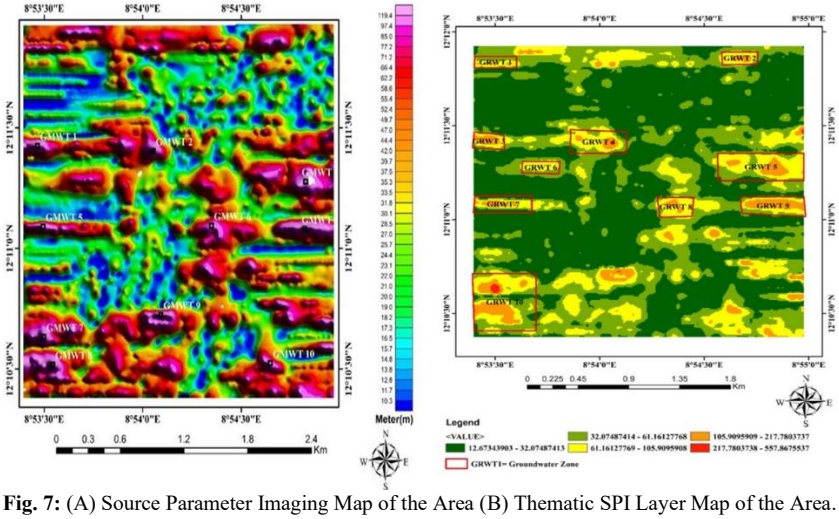


Fig. 7: (A) Source Parameter Imaging Map of the Area (B) Thematic SPI Layer Map of the Area.

Figure 7(b) shows the thematic layer of the SPI depths to the source rock; the depths are classified into five (5) regions, and each region is assigned a number from 1 to 5, as in Table 5. The first number (1) stand for very shallow depth of value ranging from 12.6743m to 32.0749m. The second number (2) is for shallow depth of value range 32.0749m to 61.1613m, the third number (3) indicates moderate depth of value range 61.1613m to 105.9096m, the forth number (4) stand for deeper depth with value range of 105.9096m to 217.7803m, and the fifth number stands for deepest depth with depth ranging from 217.7803m to 557.8675m. The thematic layer is assigned a weight of 42% (Table 4), and Table 5 shows the significance of depth in groundwater exploration.

Table 4: Aquifer Depths from Isolated Profiles Lines on the Thematic SPI Layer

SN	Profile Line	Longitude (^{0}N)	Latitude (^{0}E)	DEPTH TO AQUIFER (m)
1	GRWT 1	8.891697	12.1973	65
2	GRWT 2	8.911164	12.19766	60
3	GRWT 3	8.891133	12.1903	30
4	GRWT 4	8.899871	12.19022	200
5	GRWT 5	8.912854	12.18801	120
6	GRWT 6	8.895312	12.18796	75
7	GRWT 7	8.892288	12.18469	140
8	GRWT 8	8.906051	12.18446	125
9	GRWT 9	8.913886	12.18456	200
10	GRWT 10	8.892422	12.17602	50

3.8. Thematic elevation layer and thematic slope layer

Figure 8 (a) show the elevation thematic layer map of the study area, which were classify in to five classes. Class 1 is of very low elevation and class 5 is of very high elevation; classes 2, 3 and 4 are of low, moderate, and high elevation, respectively. This thematic layer is assigned a weight value of 7% in the groundwater potential of the study area, as shown in Table 4.

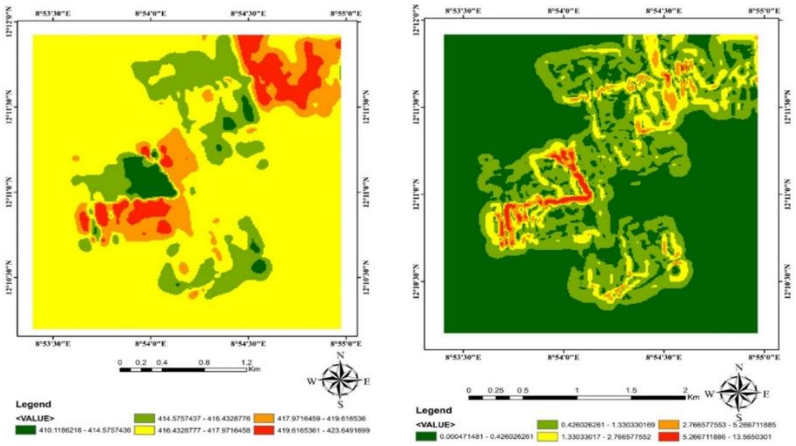


Fig. 8: (A) Thematic Elevation Layer Map of the Area. (B) Thematic Slope Layer Map of the Area

Figure 8 (b) shows the thematic layer of the slope of the area under study. The layer is categories in to five (5) classes numbered from 5 to 1, as shown in Table 4. The numbers 5, 4, 3, 2, and 1 were classified into regions of very high, high, moderate, low, and very low potential, respectively; these regions are inferred as favorable depression zones for surface water accumulation and serves as aquifer recharge zones. The thematic layer of the slope is denoted by a weight of 8% in groundwater potential.

Electromagnetic Data GRWT 1 shown in Figure 9(a) indicate a varying resistivity along the vertical and lateral distance along the profile line. The profile shows the different lithological layers around the profile.

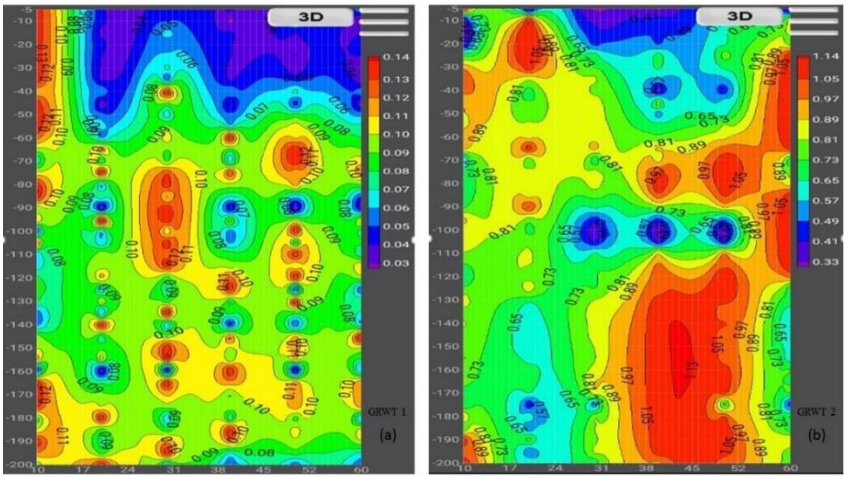


Fig. 9: (a) Typical Electromagnetic Result Pseudo-Section of GRWT1 and (b) Typical Electromagnetic Result Pseudo-Section of GRWT 2.

Four (4) layers of varying resistivity and thickness were identified around GRWT 1; topsoil which composed of silty sand followed by laterite as the second layer, the third layer composed of gravel and the forth layer is composed of sand stone of resistivity 0.03Ωm to 0.05Ωm, 0.7Ω to 0.8Ωm, 0.04Ωm to 0.05Ωm and 0.1Ωm to 0.14Ωm respectively. GRWT 2 in Figure 9(b) is predicted to have four (4) lithological layers; topsoil (silty sand), laterite, gravel and sandstone with resistivity range of 0.65Ωm to 0.81Ωm, 0.81Ωm to 0.97Ωm, and 0.33Ωm to 0.49Ωm respectively. GRWT 3 in Figure 9(c) is identified to have four (4) layers; the first layer is composed of silty sand (topsoil) with resistivity of 0.10Ωm to 0.15Ω, the second layer is composed of laterite with resistivity 0.15Ωm to 0.18Ωm, the third layer is composed of gravels with resistivity value of 0.03Ωm to 0.06Ωm and the last layer is composed of sandstone with resistivity of 0.18Ωm to 0.19Ωm.

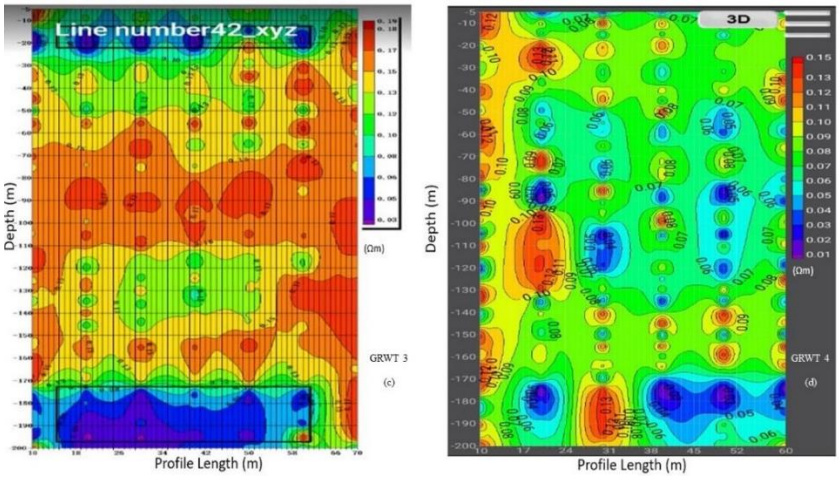


Fig. 9: (C) Typical Electromagnetic Result Pseudo-Section of GRWT3 and (D) Typical Electromagnetic Result Pseudo-Section of GRWT 4.

GRWT 4 in Figure 9(d) consists of four (4) layers. The first layer is composed of silty sand (topsoil), the second layer is composed of laterite, the third layer is made up of gravel, and the fourth layer is composed of sandstone with resistivity values ranging from 0.06 m to 0.12Ωm, 0.08Ωm to 0.13Ωm, 0.01Ωm0.04 m,.04Ωm and 0.13Ωm to 0.15Ωm. GRWT 5 in Figure 9(e) shows five variation in the litho-logical layers of the profile. The topsoil composed of silty sand is the first layer with resistivity value range of 0.09Ωm to 0.15Ωm, the second layer composed of laterite with resistivity of 0.15Ωm to 0.20Ωm, the third layer is composed of 0.04Ωm to 0.11Ωm and the forth layer is composed of sandstone of resistivity 0.17Ωm to 0.21Ωm.

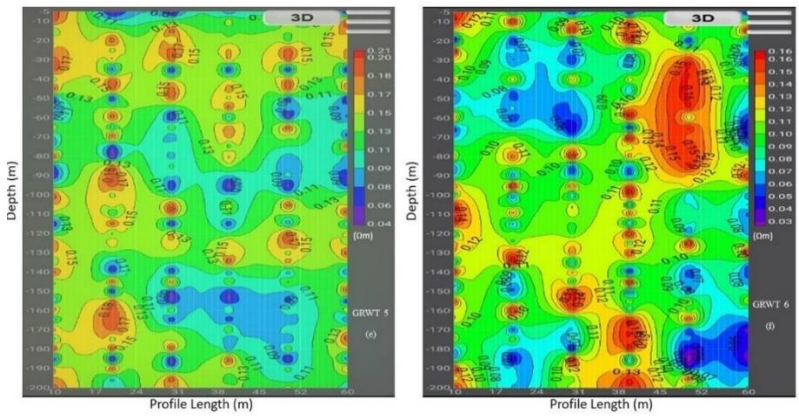


Fig. 9: (E) Typical Electromagnetic Result Pseudo-Section of GRWT 5 and (F) Typical Electromagnetic Result Pseudo-Section of GRWT 6.

GRWT 6 shown in Figure 9(f) is decomposed into four layers. These layer were identified as silty sand (topsoil), laterite (second layer), gravel (third layer), and sandstone (fourth layer) with resistivity value of 0.10Ωm to 0.15Ωm, 0.07Ωm to 0.13Ωm, 0.03Ωm to 0.07Ωm and 0.15Ωm to 0.16Ωm respectively.

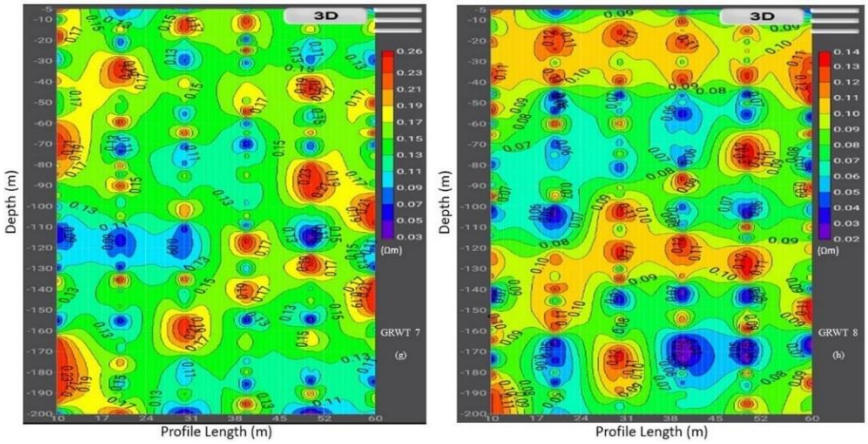


Fig. 9: (g) Typical Electromagnetic Result Pseudo-Section of GRWT 7 and (H) Typical Electromagnetic Result Pseudo-Section of GRWT 8.

Figure 9(g) shows the profile line of GRWT 7. Four layers were identified in this profile, the first layer identified is the top soil composed of silty sand with resistivity of 0.13Ωm to 0.17Ωm. the second layer is inferred as laterite with value range of 0.15Ωm to 0.23Ωm, the third layer is composed of gravel with resistivity of 0.03Ωm to 0.09Ωm. the last layer with resistivity value of 0.23Ωm to 0.26Ωm is composed of sandstone. Figure 9(h) shows a profile line of GRWT 8, which is identified as having four layers. The first layer is the topsoil (silty sand) with resistivity of 0.07Ωm to 0.09Ωm. The second layer is laterite with resistivity of 0.09Ωm to 0.13Ωm, the third layer is composed of gravels with resistivity of 0.02Ωm to 0.05Ωm and thefourthh layer is composed of sandstone with resistivity of 0.13Ωm to 0.14Ωm.

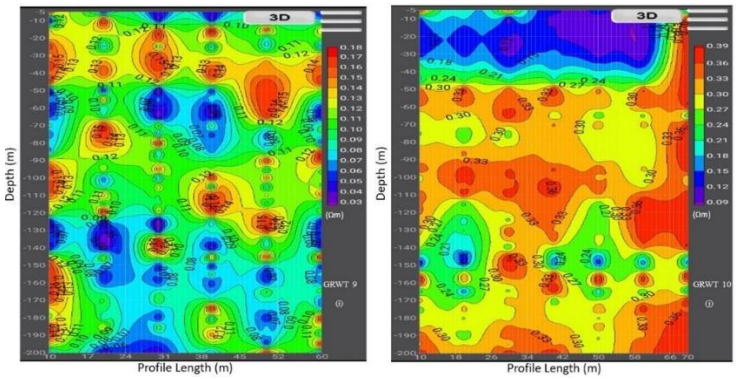


Fig. 9: (I) Typical Electromagnetic Result Pseudo-Section of GRWT 9 and (J) Typical Electromagnetic Result Pseudo-Section of GRWT 10.

GRWT 9 is presented in Figure 9(i) with profile line identified to have four layers. The layer identified as topsoil that is composed of silty sand with a resistivity of 0.07Ωm to 0.12Ωm. The second layer is composed of lateritwith a h resistivity value of 0.12Ωm to 0.17 m; the third layer is composed of gravels with a resistivity of 0.03 m.03Ωm to 0.07 m; and the forth layer is composed of sandstone with a resistivity value of 0.17Ωm to 0.18Ωm. GRWT 10 shown in Figure 9(j) shows the lithological layers around the profile line. The profile line is identified to have four layers; topsoil (silty sand), laterite, gravels and sandstone with resistivity values range of 0.21Ωm to 0.36Ωm, 0.18Ωm to 0.31Ωm, 0.09Ωm to 0.15Ωm and 0.33Ωm to 0.39Ωm. Summary of the results;is in Table 9; it shows variations in resistivity, lithological layers, and their thicknesses.

Table 5: List of Profile Location, Resistivity, Lithologies and Thickness

Profile Lines	Longitude (^{0}N)	Latitude (^{0}E)	Resistivity (Ωm) Layers			
			Silty Sand (Top-soil)	Laterite	Gravels	Sandstone
GRWT 1	8.891697	12.1973	0.03 – 0.05	0.07 – 0.08	0.04 – 0.05	0.10 – 0.14
GRWT 2	8.911164	12.19766	0.65 – 0.81	0.81 – 0.97	0.33 – 0.49	0.97 – 1.14
GRWT 3	8.891133	12.1903	0.10 – 0.15	0.15 – 0.18	0.03 – 0.06	0.18 – 0.19
GRWT 4	8.899871	12.19022	0.06 – 0.12	0.08 – 0.13	0.01 – 0.04	0.13 – 0.15
GRWT 5	8.912854	12.18801	0.09 – 0.15	0.15 – 0.20	0.04 – 0.11	0.17 – 0.21
GRWT 6	8.895312	12.18796	0.10 – 0.15	0.07 – 0.13	0.03 – 0.07	0.15 – 0.16
GRWT 7	8.892288	12.18469	0.13 – 0.17	0.15 – 0.23	0.03 – 0.09	0.23 – 0.26
GRWT 8	8.906051	12.18446	0.07 – 0.09	0.09 – 0.13	0.02 – 0.05	0.13 – 0.14
GRWT 9	8.913886	12.18456	0.07 – 0.12	0.12 – 0.17	0.03 – 0.07	0.13 – 0.18
GRWT 10	8.892422	12.17602	0.21 – 0.36	0.18 – 0.21	0.09 – 0.15	0.33 – 0.39
Thickness (m)			0 – 5	5 - 170	30 - 200	≥ 30

3.9. GWPZ of the study area

Weight overlay analysis was adopted to isolate groundwater potential zones around Gabasawa and its environs using the relative importance of the six (6) thematic layers and their subclasses. The weight allocated to each thematic layer in Table 4 is multiplied by the subclasses and subsequently summed, which gives rise to the groundwater potential zones map of the area. The GWPZ is categorized into five (5) classes. Each class is assigned a color and a number from 1–5; each class number stands for Very Low, Low, Moderate, High, and Very High potential, respectively.

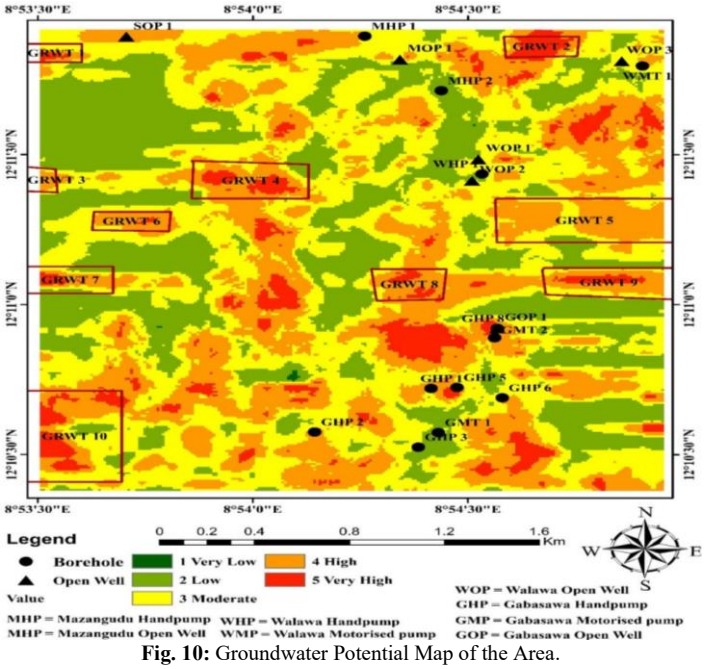


Fig. 10: Groundwater Potential Map of the Area.

Table 6: Map Area and Percentage of GWPZ of the Study Area

Class	Longitude	Latitude	Categories	Area (Km^2)	Aquifer Area Coverage (%)
1	8.901452	12.18004	Very Low	0.002430041	0.032691
2	8.902597	12.18698	Low	1.956188053	26.31629
3	8.90397	12.18569	Moderate	2.896154582	38.96152
4	8.904628	12.18507	High	2.1771694	29.28912
5	8.904738	12.18486	Very High	0.401430049	5.400376

Table 8 shows the results obtained from the GWPZ map of the study area; the results show the categories of the regions according to theory degree of potential (very high, high, moderate, low, and very low groundwater potential).
The results from the 10 profile lines shown in Table 10 revealed the area to consist of 4 layers (Figure 11); 1) silty sand with thickness of 0 – 5m, this layer is composed of dark loose sand and clay sand good for agricultural purposes, 2) laterite with thickness of 5m – 170m, 3) gravel with thickness of 30 – 200m, this have the favourable factors (low resistivity, porosity and appreciable depth is inferred as the aquiferous zone, 4) sand stone with thickness of atleast 30m (≥30), this layer is of high resistivity due to lack of factors influencing resistivity.



Fig. 11: Lithological Layers.

Table 7: Resistivity and Thickness of the Lithological Layers Around the Study Area

Layer	Materials	Resistivity (Ωm)	Thickness (m)
1	Silty Sand (Topsoil)	0.03 – 0.81	0 – 5
2	Laterite	0.07 – 0.97	5 – 10
3	Gravels	0.02 – 0.49	30 – 200
4	Sandstone	0.10 – 1.14	> 30

4. Discussion

The results from the interpretation and analysis of magnetic and elevation data are important factors in the groundwater investigation of the study area. The TMI, residual, and RTE maps of the area show a striking resemblance and are observed to have high magnetic anomalies of values ranging from 33950.8 nT to 35694.1 nT, 1795.8 nT to 4897.1 nT, and -11240.0 nT to 1255.9 nT, respectively, in the NE, SE, and SW regions of the area. Intermediate to low anomaly zones with a value range of 19484.6 nT to 31411.2 nT, -11240.0 nT to 1255.9 nT, and -8102.6 nT to 948.2 nT are seen around the NE, SE, and SW regions of the study area. These sudden changes or discontinuities in the magnetic intensity in the geological formation give rise to lineaments (faults/fractures) or regions of peaks and depressions. These regions with appreciable lineaments (faults/fractures) and favorable depressions observed in the NE and SW of the area are inferred as regions of high groundwater potential. The presence of predominant lineaments at the NE and SW locations showed a tendency for surface water accumulation and groundwater storage. The SPI results was observed to three categories of depth; the deeper depth region with depth value ranging from 42.0m to 120.1m, intermediate depth of value range 17.3 to 39.6m and shallow depth with depth range 10.3m to 16.4m. Deeper depth regions are inferred as regions of high groundwater potential due to unbalanced forces explained by Bernoulli's principle [31]. These regions were observed in the NE, SE, NW, and SW areas; intermediate depth areas are viewed around the deeper depth regions, while shallow depth areas were also observed in the NE, SE, NW, and SW regions of the study area and are isolated for groundwater exploration as shown in Table 7. The surface water was observed to flow toward the NE, SE, and SW areas of the study area due to a low elevation of 410.1186m to 416.4329m above sea level and a gentle slope of 0.0004715^0 to 1.3303^0; these regions are inferred as surface water accumulation zones. Regions indicated in Table 7 were subjected to further investigation using the electromagnetic method. The results from the electromagnetic data showed that the area is underlain by four lithological layers. The first layer, with resistivity values ranging from 0.03Ωm to 0.81Ωm and a thickness varies between 0 and 5 m is inferred as topsoil composed of silty sand. The layer is observed to be loose soil, which allows easy water penetration. The second layer composed of laterite, with resistivity value of 0.07 Ωm to 0.97 Ωm and thickness ranging from a depth of 5m to 10m. The third layer is composed of gravel with resistivity range of 0.70 Ωm to 0.49 Ωm and thickness range of 30 m to 200 m. this layer with low resistivity, appreciable thickness and porosity is inferred to be an aquiferous layer. The fourth layer with resistivity value range of 0.10 Ωm to 1.14 Ωm and thickness of at least 30 m (≥ 30 m) composed of sand stone, this layer is of high resistivity due to lack of factors influencing resistivity, the layer serves as a barrier and aid groundwater accumulation.

Very High potential zones are characterized by appreciable depth and fracturing coupled with gentle slope and elevation, which aid surface water and groundwater accumulation. Area of very high groundwater covers of to 0.4014km^2, which is about 5% of the total area. High groundwater potential also shows good factor (favorable depth, fractures, gentle slope, and elevation) for groundwater accumulation. The region has an area coverage of 2.1772km^2, which is approximately 29.2891% of the total area. The area of moderate potential has a coverage of 2.8962km^2 which about 38.9615% of the area coverage, this area also has favorable groundwater accumulation factors. Low potential area covering 1.9562km^2 that contributed 26.3163% lack appreciable factor for groundwater accumulation. Very low potential region covering an area of 0.0024km^2 that is about 0.0327% lacks good factors for groundwater accumulation as shown in Table 8. The results in this work are consistent with the prediction of [32]: [33]

5. Validation of Groundwater Potential Zone Map

Validation of the GWPZ map was made by plotting the coordinates of the existing borehole, open-well and aquifer delineated from EM analysis to affirm the potentiality of the isolated regions. However, 66.67% of the open wells are within the regions of moderate potential, 16.67% is within the very high potential region and 16.67% is within the high potential region. 16.67% and 33.33% of the boreholes fall within very high to high potential, respectively, while 33.33% and 16.67% of the boreholes are within the moderate and low groundwater potential, respectively. 100% of the ten (10) isolated aquifers from the EM analysis (GRWT 1 to GRWT 10) fall within very high to high groundwater potential zones. In comparison to the deductions of [34]: [35]. This indicates a very high level of accuracy in the prediction of GWPZ. This high percentage of agreement may be a result of contributions from the SPI, lineaments, and the Lineament Intersection, which have not been integrated in previous works.

6. Conclusions

The results from surface magnetic, elevation, electromagnetic, and hydrogeological data shown in this paper indicate that the variation in the magnetic and elevation anomalies presents an undulating topography with high values in the NE, SE, and SW regions, with patches of lower anomalies in the same regions as in high anomalies. This discontinuities in rock anomalies and surface topography give rise to lineaments, fractures and faults observed to be predominant in the NE and SW locations which have high tendency for groundwater accumulation. The results SPI map concludes that there exist regions of high, intermediate and shallow depths of 42.0m to 120.1m, 17.3m to 39.6m and 10.3m to 16.4m respectively. By comparing the lineaments and the SPI maps, it is potent to say that the deeper and intermediate regions of the area are of high groundwater potential. AHP using the MCDA process was applied to SPI, magnetic lineaments density, elevation lineament density, lineaments intersection density, elevation and slope thematic layer maps to calculate the weight for each thematic layer; the weight overlay analysis function in ArcGIS was use to multiply the weight of the thematic layer by the subclass of the respective thematic layer. The products obtained were summed up, and the GWPZ map was obtained. The GWPZ map show that very high potential has an area coverage of 0.4041 km^2 (5%), high potential has an area coverage of 2.1772 km^2 (29.29%), moderate potential has an area coverage of 2.8962 km^2 (38.9615%), low potential has an area coverage of 1.9562 km^2 (26.3163%) regions of very low potential covers an area of 0.0024 km^2 (0.0327%). Borehole, open-well, and EM data were acquired and used for GWPZ validation. The EM data were interpreted and analyzed, from the analysis, four lithological layers were delineated with varying resistivities and thicknesses around the area. The third layer composed of gravels is inferred as aquifer with high ground water potentiality. The aquifer zones delineated were georeferenced and plotted on the GWPZ map together with the borehole and open well. The plotted points show that 92.86% of the points fall within the very high to moderate groundwater potential zone on the GWPZ map.

References

[1] K. O. Musa, A. Ibrahim, G. O. Aigbadon, E. O. Akudo, O. Akakuru, F. A. Akpah, J. B. Jimoh, M. Adegbola and M. B. Aminu, "Integration of geological and geophysical techniques in groundwater mapping within Lokoja – Jakura schist belt, North Central, Nigeria," World Journal of Engineering, vol. 22, no. 2, pp. 461-479, 2025. https://doi.org/10.1108/WJE-04-2024-0187.

[2] F. O. Akinluyi, G. A. Adeyemi and M. O. Olorunfemi, "Application of multi-criteria decision analysis (MCDA) and GIS for groundwater potential mapping in the basement complex terrain of Ekiti State, southwestern Nigeria," Heliyon, vol. 7, no. 8, 2021. https://doi.org/10.1007/s40899-020-00486-5.

[3] S. A. Suleiman and M. A. Y. Hotoro, "An integrated aeromagnetic and resistivity investigation of groundwater in Tarauni Local Government Area, Kano state, Nigeria," Journal of Basic and Applied Sciences Research, pp. 45-62, 2026.

[4] National Population Commission, "Nigeria demographic and health survey 2022," NPC, 2023.

[5] D. N. Obiora, A. E. Ukatu and G. Z. Ugwu, "Aeromagnetic mapping of basement topography and lineaments for groundwater exploration in parts of the Nigerian basement complex," Journal of Applied Geophysics, vol. 192, 2021.

[6] C. C. Okpoli and A. A. Oyedele, "Structural controls on groundwater occurrence in crystalline basement aquifers of southwestern Nigeria: Insights from integrated geophysical and remote sensing studies," Hydrogeology Journal, vol. 30, pp. 1845-1867, 2022.

[7] T. A. Adagunodo, A. Adefehinti and K. D. Oyeyemi, "Groundwater potential mapping using geophysical and remote sensing techniques in the basement complex terrain of Ondo State, Nigeria.," Groundwater for Sustainable Development, vol. 14, 2021.

[8] [8] A. I. Olayinka and M. A. Olayiwola, "Electrical resistivity imaging for groundwater exploration in basement complex areas: Success rates and best practices," Near Surface Geophysics, vol. 21, no. 4, pp. 401-418, 2023.

[9] UNICEF, "Water, sanitation and hygiene in Nigeria: Situation analysis and strategic priorities," United Nations Children's Fund, 2024.

[10] Geological Survey of Nigeria Agency, "Geological map of Kano State (1:250,000 scale)," GSNA Press, 2020.

[11] Nigerian Meteorological Agency, "Climate profile of Kano State 2020–2024," NiMet Publications, 2025.

[12] M. Abubakar and A. B. Yusuf, "Climate variability and groundwater recharge dynamics in semi-arid basement complex terrains of northwestern Nigeria," Journal of African Earth Sciences, vol. 210, 2024.

[13] Z. A. Usman, S. Umar and G. K. Adamu, "Land use/land cover change and its implications for groundwater recharge in the Kano region, northern Nigeria," Environmental Earth Sciences, vol. 81, no. 234, 2022.

[14] Kano State Bureau of Statistics, "Statistical yearbook of Kano State 2024," Government of Kano State, 2025.

[15] K. O. Ibrahim, K. M. Lawal and A. Suleiman, "Integrated geophysical approach for borehole siting in crystalline basement terrains: A case study of Gabasawa area, Kano State," Nigerian Journal of Geology and Geophysics, vol. 8, no. 2, pp. 112-128, 2023.

[16] A. M. Bello, N. K. Abdullahi and H. Musa, "Challenges of rural water supply in basement complex areas of Kano State: A community-based assessment," Journal of Water, Sanitation and Hygiene for Development, vol. 14, no. 3, pp. 456-472, 2024.

[17] I. M. Sulaiman, M. L. Garba and B. Yusuf, "Traditional versus geophysical approaches to borehole siting in rural Kano State: An assessment of outcomes and cost-effectiveness," African Journal of Environmental Science and Technology, vol. 16, no. 5, pp. 178-192, 2022.

[18] O. T. Ogunribido, M. I. Oladapo and A. O. Fajana, "Geophysical methods for groundwater exploration in basement complex terrains: A review of Nigerian case studies," Journal of African Earth Sciences, vol. 198, 2023.
[19] L. R. D. Nalibrata and L. M. Jaelani, "Analysis of groundwater level dynamics in response to seasonal meteorological conditions using integrated 2D resistivity profiling and ADMT method: A case study of Surabaya City," IOP Conference Series: Earth and Environmental Science, vol. 1607, 2026. https://doi.org/10.1088/1755-1315/1607/1/012003.
[20] A. G. Tahir, M. L. Garba and I. Hamidu, "Hydrology and Groundwater Quality of Deep and Shallow Boreholes in Kano Metropolis, Northwestern Nigeria," Journal of Environment and Earth Sciences, vol. 5, no. 1, pp. 160-166, 2015.
[21] A. Hotoro, A. Alhassan and M. Ali, "Evaluation of Groundwater Potential Using Electrical Sounding Technique at the General Hospital Wudil, Kano State, Nigeria," Journal of Applied Physics (IOSR-JAP), 2022.
[22] W. Lowrie, Fundamentals of Geophysics, First Edition ed., Cambridge: Cambridge University Press, 1997, pp. 225-226.
[23] W. Telford, L. Geldart and R. Shariff, Applied Geophysics, second Edition ed., Cambridge: Cambridge University Press, 1990.
[24] S. I. Ibeneme, I. A. Oha, N. N. Abdulsalam and M. K. Onuoha, "Improved Mapping of the Structural Disposition of SomeYounger Granite Ring Complexes of Nigeria Using High Resolution Aeromagnetic Data.," J Geol Geophys, vol. 7, no. 443, pp. 1-13, 2018.
[25] T. L. Saaty, "A Scaling Method for Priorities in Hierarchical Structures," Journal of Mathematical Psycology, vol. 15, pp. 234-281, 1977. https://doi.org/10.1016/0022-2496(77)90033-5.
[26] T. L. Saaty, "Decision making with the analytic hierarchy process," Int. J. Services Sciences, vol. 1, no. 1, pp. 83-98, 2008. https://doi.org/10.1504/IJSSCI.2008.017590.
[27] T. Saranya and S. Saravanan, "Groundwater potential zone mapping using analytical hierarchy process (AHP) and GIS for Kancheepuram District, Tamilnadu, India," Modeling Earth Systems and Environment, 2020. https://doi.org/10.1007/s40808-020-00744-7.
[28] F. Echogdali, S. Boutaleb, A. Bendarma, M. Saidi, M. Aadraoui, M. Abioui, M. Ouchchen, K. Abdelrahman, M. Fnais and K. Sajinkumar, "Application of Analytical Hierarchy Process and Geophysical Method for Groundwater Potential Mapping in the Tata Basin, Morocco.," Water, vol. 14, no. 2393, pp. 1-21, 2022. https://doi.org/10.3390/w14152393
[29] Shanghai Aidu Intellegent Detection Technology Co. Ltd, "Aidu Exploration and Foundry Model," Minhang, 2025.
[30] D. H. A. Feujio, Z. Aretouyap, S. C. Tchato, C. N. I. Legrand, E. Djomdi, N. N. Madadjeu, C. N. Nguimgo and A. N. Kpoumie, "Application of analytical hierarchy process to assess groundwater potential for a sustainable management in the Menoua Division," Heliyon, vol. 10, pp. 1-17, 2024. https://doi.org/10.1016/j.heliyon.2024.e24310.
[31] Princeton University, "Bicycle_web," 14 January 2026. [Online]. Available: www.princeton.edu/~asmits/Bicycle_web/Bernoulli.html.
[32] M. M. Maina and I. Tudunwada, "Lineament Mapping for Groundwater Exploration in Kano State, Nigeria," Int'l Journal of Advances in Agricultural & Environmental Engg. (IJAAEE), vol. 4, no. 1, pp. 226-229, 2017.
[33] I. Mallam, A. O. Amoo, D. A. Umar, S. U. Usman and H. M. Gebbe, "GROUNDWATER AVAILABILITY AND AQUIFER PROPERTIES IN JIGAWA STATE: A GIS AND REMOTE SENSING APPROACH," FUDMA Journal of Sciences (FJS), vol. 9, no. 6, pp. 165-174, 2025. https://doi.org/10.33003/fjs-2025-0906-3590.
[34] O. S. Ilugbo, I. Aigbedion, O. K. Ozegin and A. M. Bawallah, "Assessment of Groundwater Occurrence in a Typical Schist Belt Region in Osun State, Southwestern Nigeria using VES, Aeromagnetic Dataset, Remotely Sensed data, GIS, and MCDA Approaches," Research Square, 2022. https://doi.org/10.21203/rs.3.rs-1649269/v1
[35] S. O. Ilugbo, I. Aigbedion and K. O. Ozegin, "Structural mapping for groundwater occurrence using remote sensing and geophysical data in Ilesha Schist Belt, Southwestern Nigeria," GEOLOGY, ECOLOGY, AND LANDSCAPES, 2023. https://doi.org/10.1080/24749508.2023.2182063
[36] R. Oghonyon, K. Itiowe, V. Okereke and D. C. Maxwell, "Subsurface Depth Delineation for Aquifer Prospecting at Redeemed Church Field, Choba, River State," International Journal of Advances in Engineering and Management (IJAEM), vol. 7, no. 9, pp. 1-11, 2025. https://doi.org/10.35629/5252-0709476485.